The Energy-Time Uncertainty Principle and the EPR Paradox: Experiments involving Correlated Two-Photon Emission in Parametric Down-Conversion*

Raymond Y. Chiao, Paul G. Kwiat, and Aephraim M. Steinberg
Department of Physics, University of California, Berkeley, CA 94720

ABSTRACT

The energy-time uncertainty principle is on a different footing than the momentum-position uncertainty principle: In contrast to position, time is a c-number parameter, and not an operator. As Aharonov and Bohm have pointed out, this leads to different interpretations of the two uncertainty principles. In particular, one must distinguish between an *inner* and an *outer* time in the definition of the spread in time Δt. It is the *inner* time which enters the energy-time uncertainty principle. We have checked this by means of a correlated two-photon light source in which the individual energies of the two photons are broad in spectra, but in which their sum is sharp. In other words the pair of photons is in an *entangled state* of energy. By passing one member of the photon pair through a filter with width ΔE, it is observed that the other member's wave packet collapses upon coincidence detection to a duration Δt, such that $\Delta E \Delta t \approx \hbar$, where this duration Δt is an *inner* time, in the sense of Aharonov and Bohm. We have measured Δt by means of a Michelson interferometer by monitoring the visibility of the fringes seen in coincidence detection. This is a nonlocal effect, in the sense that the two photons are far away from each other when the collapse occurs. We have excluded classical-wave explanations of this effect by means of triple coincidence measurements in conjunction with a beam splitter which follows the Michelson interferometer. Since Bell's inequalities are known to be violated, we believe that it is also incorrect to interpret this experimental outcome as if *energy* were a local hidden variable, i.e., as if each photon, viewed as a particle, possessed some definite but unknown energy before its detection.

*This work was supported by ONR under grant N00014-90-J-1259.

INTRODUCTION

The momentum-position and the energy-time uncertainty principles have very similar forms:

$$\Delta p \Delta x \geq \hbar/2 , \tag{1}$$

$$\Delta E \Delta t \geq \hbar/2 . \tag{2}$$

One expects this on the basis of relativistic considerations, since both momentum-energy and position-time form four-vectors. However, in the usual formulation of quantum mechanics, there is an important difference between the two uncertainty principles, since time is not an operator but a c-number parameter, in contrast to position. Hence the standard method of derivation of the uncertainty principle for momentum and position from the fundamental commutator of quantum mechanics,

$$[p, x] = \hbar/i , \tag{3}$$

does not work for energy and time. Furthermore, in contrast to momentum, energy is a physical quantity with a definite *lower* bound. These difficulties are not merely mathematical ones, as pointed out by Aharonov and Bohm [Ref. 1]. There have also been many recent papers on this subject [Ref. 2].

Aharonov and Bohm made a distinction between *inner* and *outer* times. Inner time refers to an intrinsic time defined by the system itself, whereas outer time refers to a duration of measurement made by some external apparatus. They showed by construction of an explicit counterexample that the "usual" statement of the energy-time uncertainty principle in terms of an outer time, such as, "if the duration of a measurement by an external apparatus on a system is restricted to Δt, then there exists an uncontrollable amount of energy $\Delta E \approx \hbar/\Delta t$ imparted to the system by the apparatus," is incorrect. However, the standard example of the energy-time uncertainty principle in terms of energy broadening ΔE of an atomic energy level due to its finite lifetime τ, such that $\Delta E \approx \hbar/\tau$, is correct, but here the lifetime τ refers to an *inner* time of the system. The latter example of the energy-time uncertainty principle can be understood in terms of a *classical* Fourier analysis of a finite wave train of duration τ, i.e., $\Delta\omega \approx 1/\tau$.

Here we point out a *nonclassical* aspect of this uncertainty principle, which arises from the nonlocal collapse of the wave packet upon coincidence detection of a correlated pair of photons. The two correlated photons (conventionally called "signal" and "idler" photons) are prepared by spontaneous parametric down-conversion of a uv photon in a $\chi^{(2)}$ nonlinear crystal. When one member of this pair (the "remote" one) is detected through a filter with width $\Delta\omega$, the other member (the "nearby" one) immediately collapses into a wave packet of duration $\tau \approx 1/\Delta\omega$. If the remote filter is broad, the nearby photon wave packet becomes narrow upon collapse; if the remote filter is narrow, the

nearby wave packet becomes broad, upon coincidence detection. In this sense, there exists a nonlocal action at a distance. Hence it is closely related to the Einstein-Podolsky-Rosen paradox. The way we measured τ is to pass the nearby wave packet through a Michelson interferometer. If this wave packet overlaps with itself after reflection from the mirrors of the Michelson onto the recombining beam splitter, then there will be interference fringes detected in coincidence with the remote photon; otherwise interference fringes will not be visible. The wave packet duration thus measured is clearly an *inner* time of the system, since it is self-referential.

EXPERIMENT

In our experiment the incident light was prepared in an entangled state consisting of a pair of photons whose energies, $E_s = \hbar\omega_s$ and $E_i = \hbar\omega_i$, although individually broad in spectrum, sum up to a sharp quantity $E_p = \hbar\omega_p$ because they were produced from a single pump photon whose frequency ω_p was sharp. This entangled state is given by

$$|\psi\rangle = \int d\omega_s \, A(\omega_s) \, |1\rangle_{\omega_s} \, |1\rangle_{\omega_p - \omega_s} \qquad (4)$$

where $A(\omega_s) = A(\omega_p - \omega_s)$ is the complex probability amplitude for finding one photon with a frequency ω_s, i.e., in the n=1 Fock state $|1\rangle_{\omega_s}$, and one photon with a frequency $\omega_p - \omega_s$, i.e., in the n=1 Fock state $|1\rangle_{\omega_p - \omega_s}$. According to the standard Copenhagen interpretation, the meaning of this entangled state is that when a measurement of the energy of one photon results in a sharp value E_s, there is a sudden collapse of the wavefunction such that instantly at a distance, the other photon, no matter how remote, also possesses a sharp value of energy $E_p - E_s$. Thus energy is conserved. Entangled states, i.e., coherent sums of product states, such as the one given by Eq. (4), result in Einstein-Podolsky-Rosen-like effects which are nonclassical and nonlocal [Refs. 3-4].

We prepared the entangled state of energy, Eq. (4), by means of parametric fluorescence in the $\chi^{(2)}$ nonlinear optical crystal potassium dihydrogen phosphate (KDP), excited by a single mode ultraviolet (uv) argon ion laser operating at λ=351.1 nm [Ref. 4]. The uv laser beam was normally incident on the KDP input face. In this fluorescence process, a single uv photon with a sharp spectrum is spontaneously converted inside the crystal into two photons with broad, conjugate spectra centered at half the uv frequency, conserving energy and momentum. We employed type I phase matching, so that both signal and idler beams were horizontally polarized. The KDP crystal was 10 cm long and cut such that the c-axis was 50.3° to the normal of its input face. We selected for study idler and signal beams both centered at λ=702.2 nm which emerged at +1.5° and −1.5°, respectively, with respect to the uv beam. Coincidences in the detection of conjugate photons were then observed.

In Fig. 1, we show a schematic of the experiment. The idler photon (upper beam) was transmitted through the "remote" filter F1 to the detector D1, which was a cooled RCA C31034A-02 photomultiplier. The signal photon (lower beam) entered a Michelson interferometer, inside one arm of

which were sequentially placed two zero-order quarter waveplates Q1 and Q2. The fast axis of the first waveplate Q1 was fixed at 45° to the horizontal, while the fast axis of the second waveplate Q2 was slowly rotated by a computer-controlled stepping motor. After leaving the Michelson the signal beam impinged on a second beamsplitter B2, where it was either transmitted to detector D2 through filter F2, or reflected to detector D3 through filter F3. Filters F2 and F3 were identical: They both had a broad bandwidth of 10 nm centered at 702 nm. Detectors D2 and D3 were essentially identical to D1. Coincidences between D1 and D2 and between D1 and D3 were detected by feeding their outputs into constant fraction discriminators and coincidence detectors after appropriate delay lines. We used EGG C102B coincidence detectors with coincidence window resolutions of 1.0 ns and 2.5 ns, respectively. Also, triple coincidences between D1, D2 and D3 were detected by feeding the outputs of the two coincidence counters into a third coincidence detector (a Tektronix 11302 oscilloscope used in a counter mode). The various count rates were stored on computer every second.

Our arrangement of quarter waveplates inside the Michelson interferometer generates a geometrical (Berry-Pancharatnam) phase, proportional to the angle θ between the fast axes of the quarter wave plates. We shall not go into detail concerning this phase here, except to say that it affords a convenient way to see interference fringes without changing the difference in arm lengths of the interferometer [Ref. 5].

We took data both outside and inside the white light fringe region where the usual interference in singles detection occurs. We report here only on data taken outside this region, where the optical path length difference was at a fixed value much greater than the coherence length of the signal photons determined by the filters F2 and F3. Hence the fringe visibility seen by detectors D2 and D3 in singles detection was essentially zero.

THEORY

First we present a simplified quantum analysis of this experiment. In the Appendix, we will present a more comprehensive analysis based on Glauber's correlation functions. The state of the light after the Michelson interferometer is given by

$$|\psi\rangle_{out} = \int d\omega_s\, A(\omega_s)\, |1\rangle_{\omega_s}\, |1\rangle_{\omega_p-\omega_s}\, \frac{1}{\sqrt{2}}\left\{1 + e^{i\phi(\omega_p-\omega_s)}\right\} \qquad (5)$$

where $\phi(\omega_p - \omega_s) = 2\pi\Delta L/\lambda_{\omega_p-\omega_s} + \phi_{Berry}$ is the phase shift arising from the optical path length difference ΔL of the Michelson for the photon with frequency $\omega_p - \omega_s$, plus the Berry's phase contribution for this photon. The coincidence rate N_{12} (N_{13}) between detectors D1 and D2 (D1 and D3) is proportional to the probability of finding at the same time t one photon at detector D1 placed at $\mathbf{r}_1$, and one photon at detector D2 (D3) placed at $\mathbf{r}_2$ ($\mathbf{r}_3$). When a narrowband filter F1 centered at frequency ω_s is placed in front of the detector D1, N_{12} becomes proportional to

$$|\psi'_{out}(\mathbf{r}_1, \mathbf{r}_2, t)|^2 = |\langle \mathbf{r}_1, \mathbf{r}_2, t\,|\,\psi\rangle'_{out}|^2 \propto 1 + \cos\phi\,, \qquad (6)$$

where the prime denotes the output state after a von Neumann projection onto the eigenstate associated with the sharp frequency ω_s upon measurement. Therefore, the phase ϕ is determined at the sharp frequency $\omega_p - \omega_s$, or equivalently, the sharp energy $E_p - E_s$. In practice, the energy width depends on the bandwidth of the filter F1 in front of D1, so that the visibility of the fringes seen in coincidences should depend on the width of this *remote* filter. This fringe visibility will be high, provided that the optical path length difference of the Michelson does not exceed the coherence length of the *collapsed* signal photon wave packet, determined by F1. If a sufficiently broadband remote filter F1 is used instead, such that the optical path length difference is much greater than the coherence length of the collapsed wave packet, then the coincidence fringes should disappear.

RESULTS

In Fig. 2, we show data which confirm these predictions. In the lower trace (squares) we display the coincidence count rate between detectors D1 and D3, as a function of the angle θ between the fast axes of waveplates Q1 and Q2, when the remote filter F1 was narrow, i.e., with a bandwidth of 0.86 nm. The calculated coherence length of the collapsed signal photon wave packet (570 μm) was greater than the optical path length difference at which the Michelson was set (220 μm). The visibility of the coincidence fringes was quite high, viz., 60%±5%.* This is in contrast to the low visibility, viz., less than 2%, of the singles fringes detected by D3 alone (not shown). For comparison, in the upper trace (triangles) we display the coincidence count rate versus θ when a broad remote filter F1, i.e., one with a bandwidth of 10 nm, was substituted for the narrow one. The coherence length of the collapsed signal photon wave packet was thus only 50 μm. The coincidence fringes in this case have indeed disappeared, as predicted.

DISCUSSION

In light of the observed violations of Bell's inequalities [Ref. 6], it is incorrect to interpret these results in terms of an ensemble of conjugate signal and idler photons which possess definite, but unknown, conjugate energies before filtering and detection. Any observable, e.g., energy or momentum, should not be viewed as a local, realistic property carried by the photon *before it is actually measured.*

The function of the second beamsplitter B2 was to verify that the signal beam was composed of photons in an n=1 Fock state. In such a state, the photon, due to its indivisibility, will be either transmitted or reflected at the beamsplitter, but not both. Thus coincidences between D2 and D3 should never occur, except for rare accidental occurrences of two pairs of conjugate photons within the coincidence window. However, if the signal beam were a classical wave, then one would expect an equal division of the wave amplitude at the 50% beamsplitter, and hence frequent occurrences of

*The slightly nonsinusoidal component in Fig. 3 (lower trace) can be explained by a slight wedge in Q2, in conjunction with the fact the signal beam was incident on Q2 off center.

coincidences. An inequality, which was strongly violated in our experiment, places a lower bound on this coincidence rate for classical light (see below). This verifies the essentially n=1 Fock state nature of the light, and confirms the previous result of Hong and Mandel [Ref. 7].

The vertical arrows in Fig. 2 indicate the points at which triple coincidences were measured. Let us define the anticorrelation parameter [Ref. 8]

$$a \equiv N_{123}\, N_1 / N_{12}\, N_{13} \ , \tag{7}$$

where N_{123} is the rate of triple coincidences between detectors D1, D2 and D3, N_{12} is the rate of double coincidences between D1 and D2, N_{13} is the rate of double coincidences between D1 and D3, and N_1 is the rate of singles detections by D1 alone. The inequality $a \geq 1$ has been shown to hold for any classical wave theory [Ref. 8]. The equality $a=1$ holds for coherent states $|\alpha\rangle$, independent of their amplitude α. Since in our experiment the amplitude fluctuations in the double coincidence pulses led to a triple coincidence detection efficiency η less than unity, we should reduce the expected value of a accordingly. The modified classical inequality is $a \geq \eta$. We calibrated our triple coincidence counting system by replacing the two-photon light source by an attenuated light bulb, and measured $\eta = 0.70 \pm 0.07$. During the data run of Fig. 2 (lower trace), we measured values of a shown at the vertical arrows. The average value of a is 0.08 ± 0.04, which violates by more than thirteen standard deviations the predictions based on any classical wave theory. It is therefore incorrect to interpret these results in terms of a stochastic ensemble of classical waves, in a semiclassical theory of photoelectric detection [Ref. 9]. Classical waves with conjugate, but random, frequencies could conceivably yield the observed interference pattern, but they would also yield many more triple coincidences than were observed.

We have therefore verified the energy-time uncertainty principle for pairs of photons in essentially n=1 Fock states, in a way which excludes with very high probability any possible classical explanation. These results can be understood in terms of the nonlocal collapse of the wavefunction.

ACKNOWLEDGMENTS

We thank I. H. Deutsch for helpful discussions, J. F. Clauser, E. D. Commins and H. Nathel for the loan of electronics, and R. Tyroler for the loan of the Michelson.

APPENDIX

A more rigorous theoretical description of the experiment can be carried out within the Glauber correlation function formalism [Ref. 10]. We start with the entangled state of the down-converted light

$$|\psi\rangle = \int d\omega_s\, A(\omega_s)\, |1\rangle_{\omega_s}\, |1\rangle_{\omega_p - \omega_s} \tag{A.1}$$

where $A(\omega_s) = A(\omega_p - \omega_s)$ is the complex probability amplitude for finding one photon with a frequency ω_s and one photon with a frequency $\omega_p - \omega_s$. For simplicity we have assumed that the pump photon is monochromatic. The second order correlation function relating the field amplitudes for the signal and idler modes at the times t_s and t_i, respectively, is defined as

$$G^{(2)}(t_s,t_i;\, t_i,t_s) = \langle \psi \,|\, \hat{E}_s^{(-)}(t_s)\, \hat{E}_i^{(-)}(t_i)\, \hat{E}_i^{(+)}(t_i)\, \hat{E}_s^{(+)}(t_s) \,|\, \psi \rangle. \tag{A.2}$$

In this expression, $\hat{E}_{s(i)}^{(-)}(t_{s(i)})$ and $\hat{E}_{s(i)}^{(+)}(t_{s(i)})$ are the negative- and positive-frequency parts of the electric field for the signal (idler) mode. Assuming, as in Fig.1, that the idler photon is directed to detector D1, the field operators for this mode at the time t_i may simply be Fourier expanded in terms of a frequency-dependent detection efficiency $|\eta_1(\omega_i)|^2$, and creation and destruction operators $\hat{a}_i^\dagger(\omega_i)$ and $\hat{a}_i(\omega_i)$:

$$\hat{E}_i^{(+)}(t_i) = \int d\omega_i\, \eta_1^*(\omega_i)\, \hat{a}_i(\omega_i)\, e^{-i\omega_i t_i} \tag{A.2a}$$

$$\hat{E}_i^{(-)}(t_i) = \left(\hat{E}_i^{(+)}(t_i)\right)^\dagger. \tag{A.2b}$$

The effects of filter F1 are included in the factor η. Similarly, the signal mode field operators may be expanded, but these require an additional factor to account for the interferometer:

$$\hat{E}_s^{(+)}(t_s) = \int d\omega_s\, \eta_2^*(\omega_s)\, \hat{a}_s(\omega_s)\, e^{-i\omega_s t_s} \frac{1}{\sqrt{2}} \left\{1 - e^{i\omega_s \tau}\, e^{i\phi_B}\right\} \tag{A.3a}$$

$$\hat{E}_s^{(-)}(t_s) = \left(\hat{E}_s^{(+)}(t_s)\right)^\dagger, \tag{A.3b}$$

where $\tau = \Delta L/c$ is the optical delay time between the arms of the interferometer, and ϕ_B is the geometrical/Berry phase.

The probability of joint detection of a signal-idler pair within the detector resolution window ΔT, after a total time $\mathcal{T}$, is then given by

$$P = \int_{-\mathcal{T}/2}^{\mathcal{T}/2} dt_s \int_{t_s - \frac{\Delta T}{2}}^{t_s + \frac{\Delta T}{2}} dt_i\, G^{(2)}(t_s,t_i;t_i,t_s) \tag{A.4}$$

In practice, the duration time $\mathcal{T}$ of any data point is essentially infinite (with respect to all relevant time-scales in the problem). In addition, for our experiment ΔT ($\approx$1ns) was much greater than τ ($\approx$730fs, for ΔL=220μm) and the reciprocal bandwidths, $1/\Delta\omega_i$ and $1/\Delta\omega_s$, of the filters F1 and F2.

Hence, we are justified in setting the limits of integration to infinity:

$$P \approx \int_{-\infty}^{\infty} dt_s \int_{-\infty}^{\infty} dt_i \int d\omega \int d\omega'\, A(\omega)A^*(\omega') \int d\omega_s \int d\omega'_s \int d\omega_i \int d\omega'_i$$
$$\times\ \eta_1(\omega_i)\,\eta_1^*(\omega'_i)\,\eta_2(\omega_s)\,\eta_2^*(\omega'_s)\,e^{i(\omega_i-\omega'_i)t_i}\,e^{i(\omega_s-\omega'_s)t_s}$$
$$\times\ \frac{1}{2}\left(1-e^{-i\omega_s\tau}e^{-i\phi_B}\right)\left(1-e^{i\omega'_s\tau}e^{i\phi_B}\right)$$
$$\times\ {}_{\omega',\,\omega_p-\omega'}\langle 1,1 \mid \hat{a}_s^\dagger(\omega_s)\,\hat{a}_i^\dagger(\omega_i)\,\hat{a}_i(\omega'_i)\,\hat{a}_s(\omega'_s) \mid 1,1\rangle_{\omega,\,\omega_p-\omega} \qquad \text{(A.5)}$$

If we assume that the probability amplitude is essentially constant ($A(\omega) \approx A_0$) over the filter bandwidths $\Delta\omega_i$ and $\Delta\omega_s$, and that $\eta_2(\omega_s) \approx \eta_{20}$ over the bandwidth $\Delta\omega_s >> 1/\tau$ (i.e. a broad square bandpass filter F2 in front of detector D2), then (A.5) simplifies considerably:

$$P \approx |A_0|^2\,|\eta_{20}|^2 \int d\omega_i\,|\eta_1(\omega_i)|^2\left\{1-\cos\left[(\omega_p-\omega_i)\tau+\phi_B\right]\right\}. \qquad \text{(A.6)}$$

We now examine the behavior of this detection probability in two limiting cases of filter F1:

1. If $|\eta_1(\omega_i)|^2 \approx |\eta_{10}|^2\,\delta(\omega_i-\omega_{i0})$ (i.e. a very narrow filter in front of detector D1), then

$$P \approx |A_0|^2\,|\eta_{20}|^2\,|\eta_{10}|^2\left\{1-\cos\left[(\omega_p-\omega_{i0})\tau+\phi_B\right]\right\}. \qquad \text{(A.7)}$$

It should be clear from (A.6) that in order to observe these fringes, it suffices to have $\Delta\omega_i << 1/\tau$. This is the situation in the lower trace of Fig. 2.

2. If $|\eta_1(\omega_i)|^2 \approx |\eta_{10}|^2\,e^{-(\omega_i-\omega_{i0})^2/\Delta\omega_i^2}$, where $\Delta\omega_i >> 1/\tau$ (we have previously stipulated the experimental condition $\Delta\omega_s >> 1/\tau$), then

$$P \approx |A_0|^2\,|\eta_{20}|^2\,|\eta_{10}|^2, \qquad \text{(A.8)}$$

a constant, with no fringes. The experimental results (top trace, Fig. 2) corresponding to a broad filter F1 are in agreement with these predictions.

Note that since the filter F2 is relatively broadband (i.e. $\Delta\omega_s >> 1/\tau$), there are no fringes visible in the singles rate of detector D2, even though fringes in coincidence may be present.

REFERENCES

1. Y. Aharonov and D. Bohm, Phys. Rev. **122**, 1649 (1961).

2. P. E. Hussar, Y. S. Kim, and M. E. Noz, Am. J. Phys. **53**, 142 (1985), and references contained therein; B. A. Orfanopoulos, Phys. Essays **3**, 368 (1990).

3. M. A. Horne, A. Shimony, and A. Zeilinger, Phys. Rev. Lett. **62**, 2209 (1989).

4. P. G. Kwiat, W. A. Vareka, C. K. Hong, H. Nathel, and R. Y. Chiao, Phys. Rev. **A41**, 2910 (1990), and references therein.

5. P. G. Kwiat and R. Y. Chiao, Phys. Rev. Lett. **66**, 588 (1991).

6. J. G. Rarity and P. R. Tapster, Phys. Rev. Lett. **64**, 2495 (1990), and references therein.

7. C. K. Hong and L. Mandel, Phys. Rev. Lett. **56**, 58 (1986).

8 P. Grangier, G. Roger, and A. Aspect, Europhys. Lett. **1**, 173 (1986).

9 J. F. Clauser, Phys. Rev. **D9**, 853 (1974).

10 R. J. Glauber, Phys. Rev. **130**, 2529 (1963).

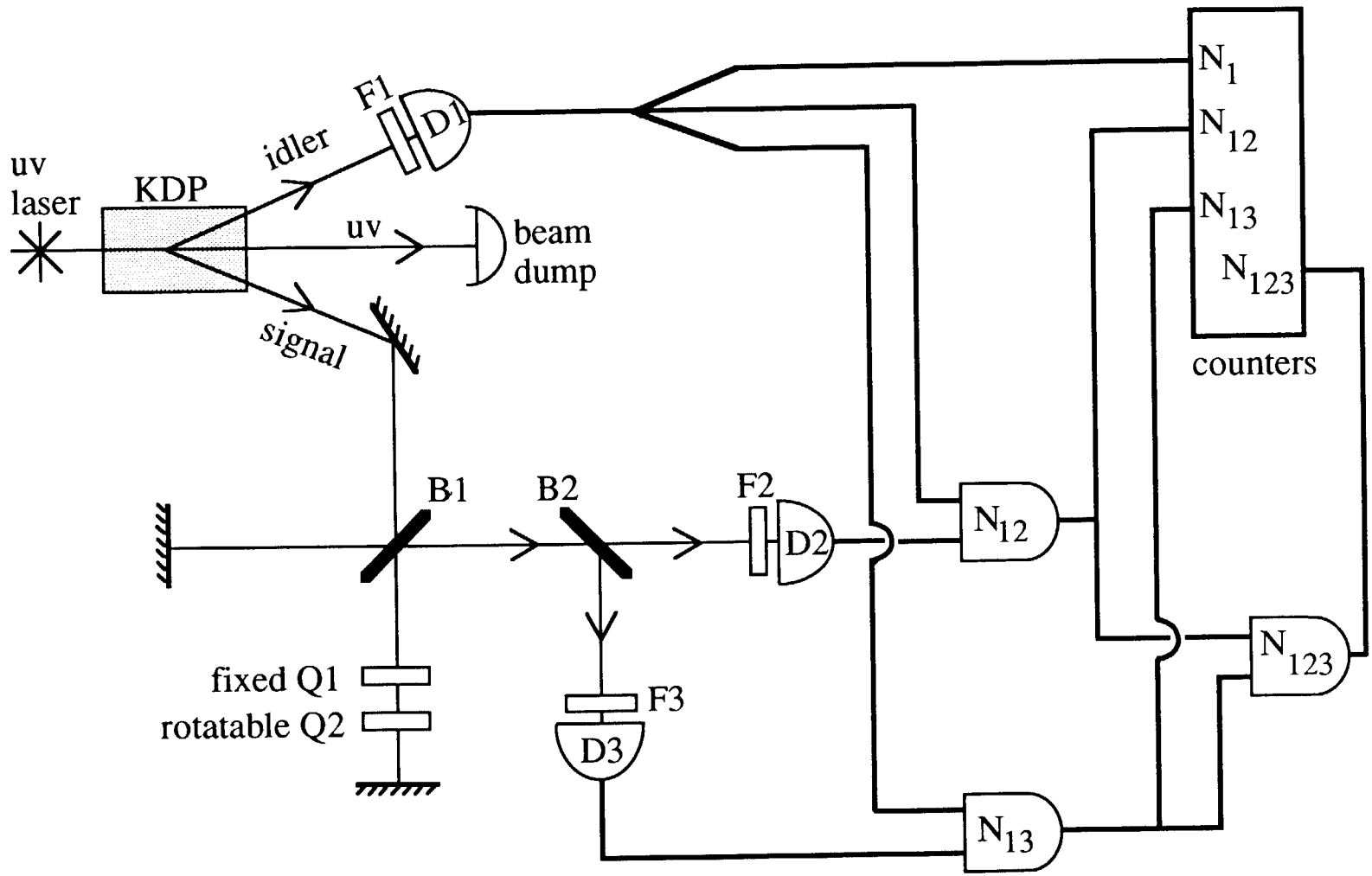

Fig. 1: Schematic of experiment to verify the energy-time uncertainty principle for correlated pairs of photons. D1, D2, and D3 are photomultipliers, Q1 and Q2 quarter waveplates, and B1 and B2 beamsplitters. Logical "AND" symbols denote coincidence detectors.

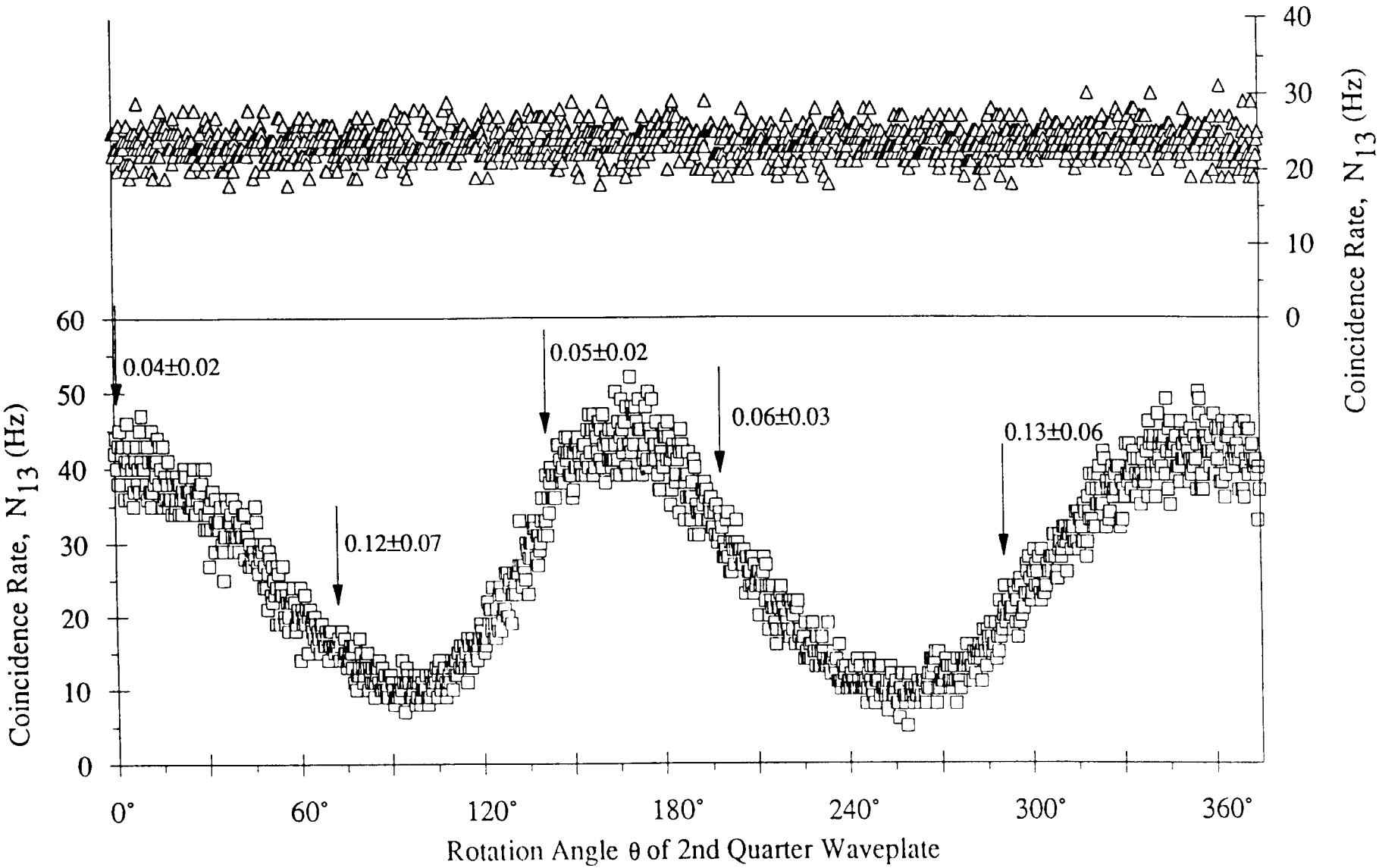

Fig. 2: Interference fringes (lower trace, squares) for an unbalanced Michelson with a slowly varying Berry's phase, observed in coincidences between D3 and D1 with a narrow remote filter F1. With a broad F1, these fringes disappear (upper trace, triangles). They also disappear when detected by D3 alone. Vertical arrows indicate where the anti-correlation parameter *a* was measured (see text).